JGR Space Physics

RESEARCH ARTICLE
10.1029/2021JA029834

Key Points:

- With a test particle model, we have quantified the proportion of beam-like electrons caused by Landau resonance with whistler waves
- The dependences of n_b / n_h on plasma conditions and wave parameters are also studied, and $E_{\|}$ plays a dominant role
- Compared with observations, the detected beam-like population can be driven by some quasi-parallel waves but is unlikely for oblique waves

Correspondence to:
X. Gao,
gaoxl@mail.ustc.edu.cn

Citation:
Kong, Z., Gao, X., Chen, H., Lu, Q., Chen, R., Ke, Y., & Wang, S. (2021). The correlation between whistler mode waves and electron beam-like distribution: Test particle simulations and THEMIS observations. *Journal of Geophysical Research: Space Physics*, *126*, e2021JA029834. https://doi.org/10.1029/2021JA029834

Received 8 MAY 2021
Accepted 28 OCT 2021

The Correlation Between Whistler Mode Waves and Electron Beam-Like Distribution: Test Particle Simulations and THEMIS Observations

Zhenyu Kong[1,2], Xinliang Gao[1,2], Huayue Chen[1,2], Quanming Lu[1,2], Rui Chen[1,2], Yangguang Ke[1,2], and Shui Wang[1,2]

[1]Department of Geophysics and Planetary Science, CAS Key Laboratory of Geospace Environment, University of Science and Technology of China, Hefei, China, [2]CAS Center for Excellence in Comparative Planetology, Hefei, China

Abstract The beam-like electron population is often observed along with whistler mode waves in the Earth's magnetosphere, but its generation mechanism is still under debate. In this study, we use a test particle simulation model to study the Landau resonance between whistler mode waves and electrons, and quantify the proportion n_b / n_h of beam-like electrons. There is a trend that the n_b / n_h first increases and then decreases with the increasing temperature of hot electrons or ratio of plasma frequency to electron gyrofrequency. While the n_b / n_h is positively correlated with the parallel electric field, magnetic amplitude, wave normal angle, or frequency of whistler mode waves if other parameters are fixed. Essentially the parallel electric field is the key parameter in determining n_b / n_h. Furthermore, we have also compared simulation results with THEMIS observations for one year. The results suggest the observed beam-like population could be generated by simultaneously observed whistler mode waves for 44.5% quasi-parallel cases. But the beam-like population is unlikely to be generated by simultaneously observed waves for the remaining 55.5% of quasi-parallel cases and nearly all oblique cases. Our study provides a better understanding of the formation of beam-like electron distribution in the Earth's magnetosphere.

1. Introduction

Whistler mode waves are significant electromagnetic waves in the Earth's magnetosphere, which is essential for regulating electron behaviors in the Van Allen radiation belts (Bortnik & Thorne, 2007; Horne, 2003; Thorne, 2010). They are considered to be the dominant cause for refilling relativistic electrons in the radiation belts during substorms (Horne & Thorne, 2003; Thorne et al., 2013) and the precipitation of electrons in the energy range from ~100 eV to ~30 keV into the Earth's atmosphere (Horne & Thorne, 2003; Ni et al., 2011; Thorne et al., 2010). Whistler mode waves fall within a typical frequency range of 0.1–0.8f_{ce} (where f_{ce} is the equatorial electron gyrofrequency), which are usually divided by a power gap around 0.5 f_{ce} into the lower and upper bands (Burtis & Helliwell, 1969; Gao et al., 2017; Li et al., 2012; Tsurutani & Smith, 1974). Whistler mode waves are mainly excited by the injected plasma sheet electrons with thermal anisotropy (Gao et al., 2014; Kennel & Petschek, 1966; Tsurutani & Smith, 1977), and their main source region locates close to the geomagnetic equator (Demekhov et al., 2017; LeDocq et al., 1998; Li et al., 2009; Lu et al., 2019). Satellite observations reveal that whistler mode waves always propagate quasi-parallel to the background magnetic field (i.e., with wave normal angles θ lower than 30°) at lower latitudes (Chen et al., 2013; Goldstein & Tsurutani., 1984). A population of very oblique waves is observed even near the equator (Agapitov et al., 2014; Li, Bortnik, et al., 2011). These chorus are often have falling tone time-frequency dependence (Li, Thorne, et al., 2011; Taubenschuss et al., 2014).

In the magnetosphere, whistler mode waves and beam-like (or plateau) electron velocity distribution are often observed simultaneously in the parallel direction with respect to the geomagnetic field lines (Agapitov et al., 2015, 2016; Li et al., 2019). With long-term THEMIS data, Min et al. (2014) showed there usually exists a beam-like electron distribution near the Landau resonant velocity (i.e., the phase velocity of whistler wave) along with the occurrence of whistler waves. Artemyev and Mourenas (2020) studied the correlation between whistler mode waves and electron beam-like components based on the energy conservation and entropy growth laws, and proposed that most of these beam-like electrons are unlikely to be caused by these simultaneously observed whistler waves. While Chen et al. (2019) found that the proportion of electron

beam-like components is proportional to the wave parallel electric field for quasi-parallel whistler waves but nearly independent for quite oblique waves. They suggested that the beam-like electrons could be resulted from the Landau resonance with quasi-parallel whistler waves, but they may be produced by other processes and provide the precondition for exciting very oblique waves. Recent studies have also proposed that the beam-like electron population plays a key role in the formation of the power gap around $0.5f_{ce}$ for whistler mode waves (Chen et al., 2020, 2021; Li et al., 2019). Omura et al. (2009) suggested that the whistler waves excited in the equatorial region will experience nonlinear damping around $0.5f_{ce}$ by the beam-like electrons (the trapped electrons) due to magnetic field inhomogeneity, as they propagate to the higher latitudes. However, so far, the correlation between whistler mode waves and beam-like electron population still remains unclear.

In this paper, we use the test particle simulation method to investigate the electron beam-like distribution formed by the Landau resonance between whistler mode waves and electrons. We have quantified the proportion of beam-like electrons caused by the Landau resonance, and studied the dependences on plasma and wave parameters. Furthermore, we also compare the simulation results with one-year THEMIS satellite observations. The paper is organized as follows. The test particle simulation method is described in Section 2. Section 3 shows the simulation results and comparison with THEMIS observations. We summarize and discuss the principal results in Section 4.

2. Test Particle Simulation Method

The interaction between the whistler mode wave and electrons is studied in a two-dimensional homogeneous simulation model. The ambient magnetic field $\mathbf{B}_0 = B_0\mathbf{e}_z$ is along the z-axis. The whistler mode wave is monochromatic and its wave number vector is lying in the (x,z) plane. The wave magnetic and electric fields are given as

$$\mathbf{B}_w = B_x^w cos\varphi\,\mathbf{e}_x + B_y^w sin\varphi\,\mathbf{e}_y - B_z^w cos\varphi\,\mathbf{e}_z, \tag{1}$$

$$\mathbf{E}_w = E_x^w sin\varphi\,\mathbf{e}_x - E_y^w cos\varphi\,\mathbf{e}_y + E_z^w sin\varphi\,\mathbf{e}_z, \tag{2}$$

where $\varphi = k_z z + k_x x - \omega t + \varphi_0$ and ω are the wave phase and frequency, and k_x and k_z are wave numbers in the x- and z-directions, respectively. It is worth noting that k_x and k_z are taken as positive, which means that the wave propagates along the positive direction of the x-axis and z-axis. The initial wave phase φ_0 is randomly chosen between 0 and 2π. The dispersion relation of whistler mode wave is obtained by the linear theory model, that is, WHAMP model (Ronnmark, 1982), which is controlled by the ratio between plasma frequency and electron gyrofrequency $\omega_{pe} / \Omega_{ce}$ (where $\omega_{pe} = \sqrt{n_0 e^2 / m_e \varepsilon_0}$ is the plasma frequency and $\Omega_{ce} = eB_0 / m_e$ is the electron gyrofrequency), the number density of hot electrons n_h / n_0 (where n_0 is the total plasma density), and the wave normal angle θ. For a chosen ω, the wave amplitudes (B_i^w and E_i^w, where the subscripts $i = x$, y, and z, are the absolute values of the complex amplitude) and the wave numbers (k_x and k_z) are obtained from the WHAMP model. Notably, the wave is injected at the very beginning, and the frequency, wave vector, and amplitudes are treated as constant in the entire simulation.

In our simulation model, a population of test electrons with a Maxwellian distribution is employed, whose number density is n_h. The particles move in the (x,z) plane, while their full velocity vectors (v_x, v_y, v_z) are updated in the calculation. The electron motion is described in Appendix A.

The sizes of the simulation area are $x = 5\lambda_x$ and $z = 5\lambda_z$ (where λ_x and λ_z are wave wavelengths in the x- and z-directions, and $\lambda_i = 2\pi / k_i (i = x,z)$), and the size of the grid cell is $\Delta x = \Delta z = 0.18 V_{Ae}\Omega_{ce}^{-1}$ (where $V_{Ae} = B_0 / \sqrt{\mu_0 n_0 m_e}$ is the electron Alfven speed). It is worth noting that the grid cell is employed here just for the convenience of analyzing the electron velocity distribution. There are, on average, 100 macro-particles in every cell. The time step is $\Delta t = 0.02\Omega_{ce}^{-1}$. The periodic boundary conditions are used along the x-direction and z-direction.

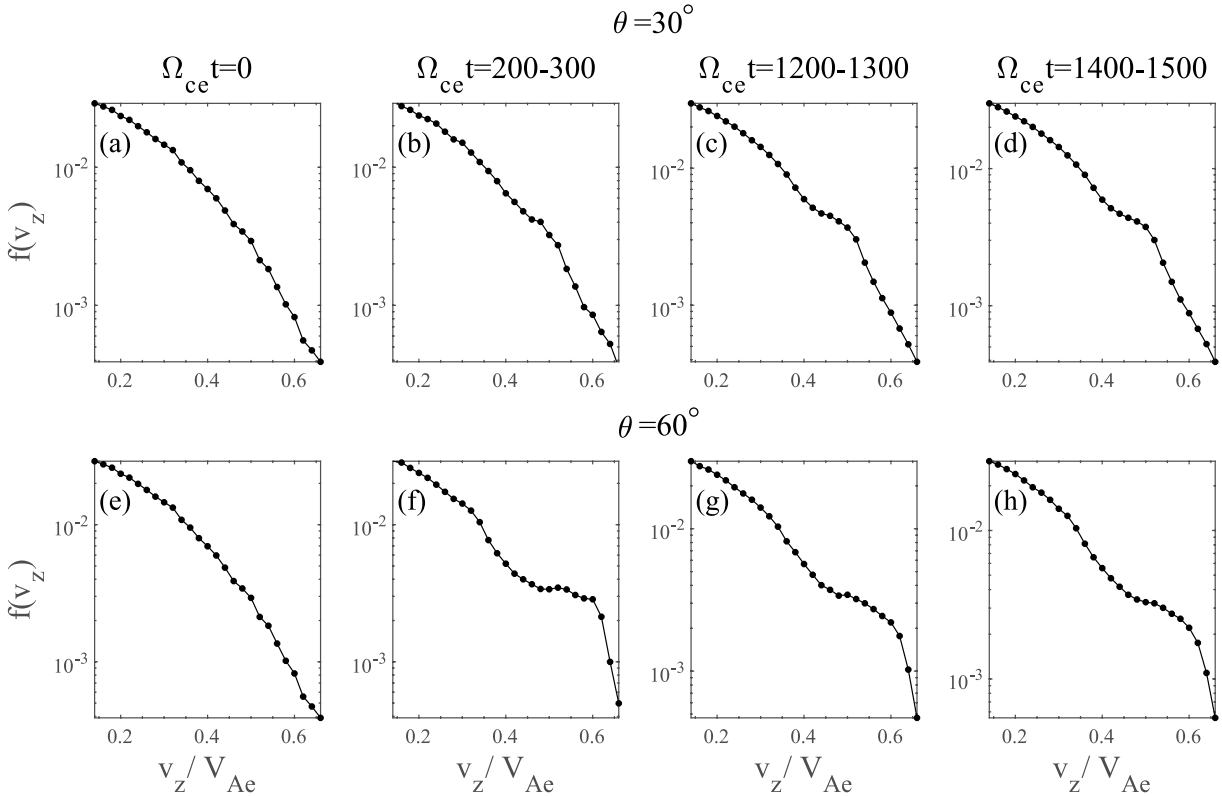

Figure 1. The electron parallel velocity distribution in Case 1 at (a) $\Omega_{ce}t = 0$, and during (b) $\Omega_{ce}t = 200 - 300$, (c) $\Omega_{ce}t = 1200 - 1300$, and (d) $\Omega_{ce}t = 1400 - 1500$. (e–h) The parallel velocity distributions in Case 2 during the same time periods.

3. Simulation Results

Two cases are chosen to show how to calculate the proportion of beam-like electrons caused by the Landau resonance in our test particle simulations. In both cases, the background magnetic field and total plasma density are assumed to be $B_0 = 144$ nT and $n_0 = 5\,\mathrm{cm}^{-3}$ (the typical values at $L = 6$ in the Earth's magnetosphere), leading to the ratio between the plasma frequency and electron gyrofrequency as $\omega_{pe} / \Omega_{ce} = 5.0$. The number density of hot electrons is set as $n_h / n_0 = 0.01$, and their thermal velocity is initialized as $v_{th} = 0.31V_{Ae}$ corresponding to the temperature of $T_h = 1keV$. A monochromatic whistler mode wave is employed in two cases, whose wave frequency ω and amplitude δB are set as $0.25\Omega_{ce}$ and $0.01B_0$, respectively. In Case 1, the wave normal angle is fixed at $\theta = 30^\circ$ (i.e., quasi-parallel), while the wave normal angle is fixed as $\theta = 60^\circ$ (i.e., very oblique) in Case 2.

Figure 1 shows the evolution of the parallel velocity distribution of hot electrons in two cases. In Case 1, the initial velocity distribution of hot electrons satisfies a Maxwellian distribution as shown in Figure 1a. Due to the Landau resonance with the whistler mode wave, a beam-like population at $\sim 0.5V_{Ae}$ appears at $\Omega_{ce}t = 200 - 300$ (Figure 1b) and becomes more distinct at $\Omega_{ce}t = 1200 - 1300$ (Figure 1c). Afterward, the velocity distribution nearly remains unchanged (Figure 1d), suggesting the beam-like population has reached saturation. Note that the saturation time is quite short, corresponding to ~0.05 s in the Earth's magnetosphere. The evolution of electron parallel distribution in Case 2 is quite similar to Case 1 except that the beam-like population at $\sim 0.5V_{Ae}$ is more significant in Case 2.

We also estimate the proportion of the beam-like population in each case. Figure 2 displays the velocity distributions at $\Omega_{ce}t = 1400 - 1500$ in (a) Case 1 and (b) Case 2, which are denoted by black dots. The Landau resonant velocities have been marked by blue dashed lines, which are estimated by $v_L = \omega / k_z$. In Case 1, $v_L = 0.45V_{Ae}$, and in Case 2, $v_L = 0.50V_{Ae}$. Note that the time is chosen because the beam-like population reaches saturation. Then, we fit the velocity distribution function around the Landau resonant velocity by

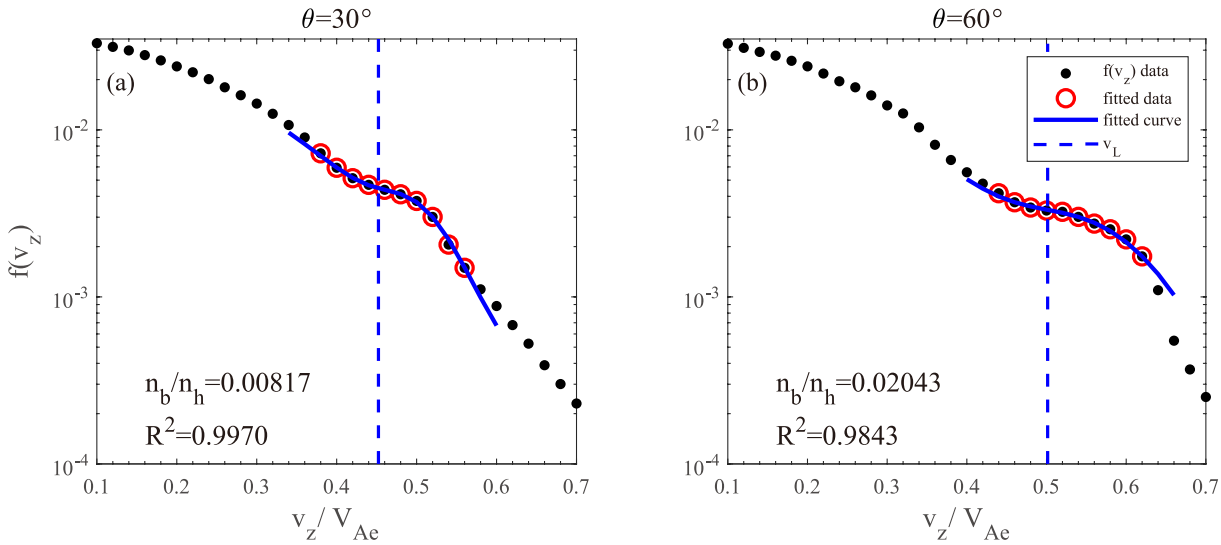

Figure 2. The parallel velocity distributions of hot electrons during $\Omega_{ce}t$ =1400 − 1500 in (a) Case 1 and (b) Case 2. The black dots are simulation results, while 10 of them spotted by red cycles are selected for fitting. The blue line is corresponding multicomponent fits. The vertical blue dashed line represents the Landau resonant velocity.

choosing 10 data points (red circles) and assume the distribution contains two electron components (i.e., hot and beam-like populations):

$$f_e = f_h + f_b = n_h\left(\frac{m}{2\pi T_h}\right)^{\frac{1}{2}}\exp\left(-m\frac{v_z^2}{2T_h}\right) + n_b\left(\frac{m}{2\pi T_b}\right)^{\frac{1}{2}}\exp\left(-m\frac{\left(v_z - v_d\right)^2}{2T_b}\right), \tag{3}$$

where T_j and n_j ($j = h$ or b) are the temperature and the number density of j component and v_d is the bulk velocity of the beam-like population. We have fitted the simulated distribution function (see Appendix B). The fitted curves are plotted as blue lines in Figure 2.

We first investigate how the proportion of beam electrons depends on the initial plasma conditions. A series of simulation runs are performed with various initial temperatures (from 0.5 to 10 keV) of hot electrons but keeping other parameters the same as those in Case 1 and Case 2. Figure 3a illustrates the dependence of

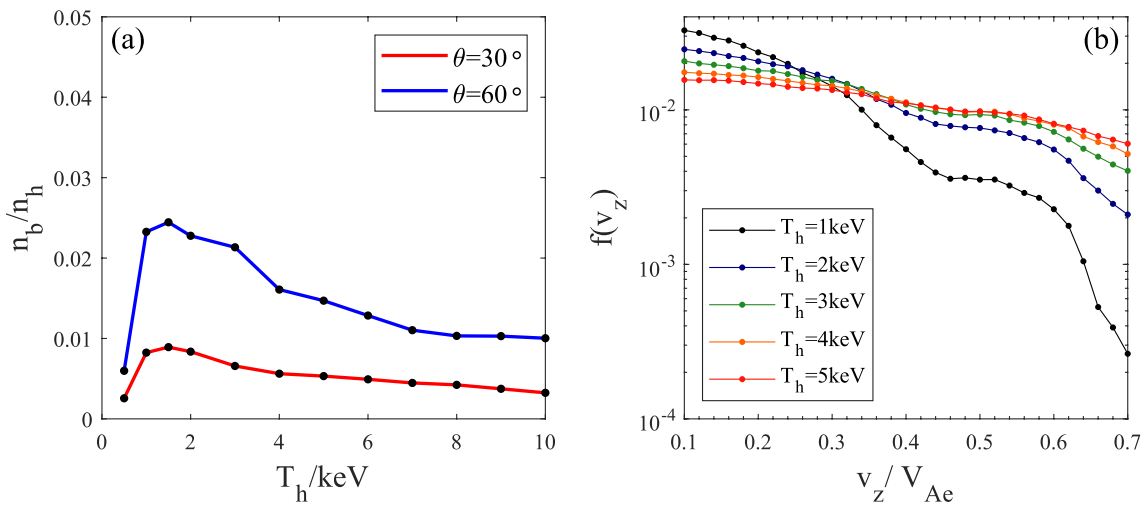

Figure 3. (a) Dependence of the estimated n_b / n_h on T_h for the quasi-parallel (θ = 30°; red line) and oblique (θ = 60°; blue line) whistler mode waves, respectively. (b) The parallel velocity distribution of the cases with θ = 60° and T_h = 1, 2, 3, 4, and 5 keV.

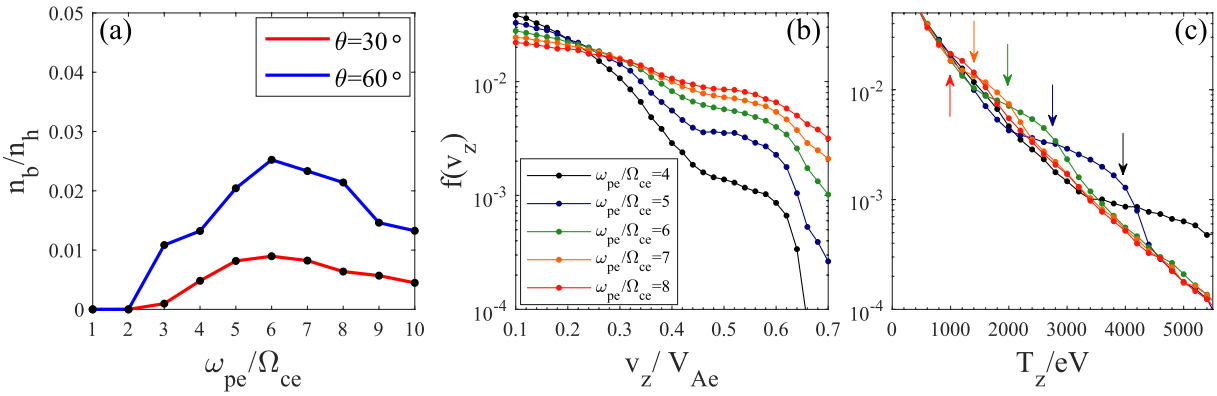

Figure 4. (a) Dependence of the estimated n_b / n_h on ω_{pe} / Ω_{ce} for the quasi-parallel (θ = 30°) and oblique waves (θ = 60°), which are represented by red and blue lines, respectively. (b) The electron parallel velocity distributions as a function of v_z / V_{Ae} for θ = 60° with ω_{pe} / Ω_{ce} = 4, 5, 6, 7, and 8. (c) The electron parallel velocity distribution as a function of parallel energy (T_z) for θ = 60° with ω_{pe} / Ω_{ce} = 4, 5, 6, 7, and 8. The resonant energies in each case are denoted by arrows in different colors.

the estimated n_b / n_h on T_h for the quasi-parallel (θ = 30°; red line) and oblique (θ = 60°; blue line) whistler mode waves, respectively. Generally, the oblique whistler mode wave can produce more beam-like electrons than the quasi-parallel wave if they have the same magnetic amplitude (Figure 3a). As shown in Figure 3a, for the quasi-parallel or oblique wave, the n_b / n_h starts to increase with the T_h and then decreases, leading to n_b / n_h peaking at T_h = 1.5 keV. For θ = 60°, the peak value of n_b / n_h is about 0.0245 and about 0.0089 for θ = 30°. To better understand the correlation between n_b / n_h and T_h, we have displayed the parallel velocity distributions for θ = 60° with different T_h in Figure 3b. For smaller T_h (<1.5 keV), the beam-like population becomes more evident with the increasing T_h since more electrons satisfy the Landau resonance condition with the whistler mode wave. However, for very large T_h (>1.5 keV), the velocity distribution of hot electrons is too flat to form the beam-like (or plateau) structure, so the estimated proportion is declining with T_h.

The influence of ω_{pe} / Ω_{ce} on the proportion of beam-like electrons is studied by performing a series of cases with ω_{pe} / Ω_{ce} = 1–10. Figure 4a shows the dependence of the estimated n_b / n_h on ω_{pe} / Ω_{ce} for the quasi-parallel (θ = 30°) and oblique waves (θ = 60°), which are represented by red and blue lines, respectively. Again, the oblique whistler mode wave still produces more beam-like electrons. Moreover, with the increasing ω_{pe} / Ω_{ce}, the estimated proportion n_b / n_h first increases, then decreases, peaking at ω_{pe} / Ω_{ce} = 6 for both quasi-parallel and oblique cases. For the case with θ = 30°, the peaking n_b / n_h is ~0.0089, and ~0.0252 for θ = 60°. Figure 4b displays the parallel velocity distributions as a function of v_z / V_{Ae} for θ = 60° with different ω_{pe} / Ω_{ce}. However, to better understand the trend in Figure 4a, we further plot the velocity distribution as a function of parallel energy (T_z) in Figure 4c, in which the resonant energies in each case are denoted by arrows in different colors. Here, we assume the background magnetic field to be fixed, so the increasing ω_{pe} / Ω_{ce} denotes the increasing plasma density. Since the initial electron velocity distribution remains same in these cases, then the Landau resonant velocity (arrow) decreases as the ω_{pe} / Ω_{ce} increases. For smaller ω_{pe} / Ω_{ce} (<6), there are more electrons resonant with the whistler mode wave as the resonant velocity moves to smaller values, and then the beam-like shapes become more obvious. While, for larger ω_{pe} / Ω_{ce} (>6), the beam-like shape becomes weaker as ω_{pe} / Ω_{ce} increases, since the velocity distribution below T_z = 2 keV is too flat.

We have also investigated the dependences of n_b / n_h on the wave properties. Here, we have performed a series of cases with the various wave normal angles θ (from 10° to 70°) but the constant wave amplitude [either $\delta E_{\parallel}$ / $\left(B_0 V_{Ae}\right)$ or δB / B_0]. Based on the linear theory, the electrostatic component [$\delta E_{\parallel}$ / $\left(B_0 V_{Ae}\right)$] of whistler mode wave will become stronger with the θ if δB / B_0 is fixed. Therefore, the acceleration due to the Landau resonance will become more efficient with the increasing θ values. Just as shown in Figure 5a, the n_b / n_h increases significantly as with θ (red line). The velocity distributions of the cases with θ = 30° – 70° are displayed in Figure 5b, in which the more significant beam-like population is observed for the larger θ. While, when the $\delta E_{\parallel}$ / $\left(B_0 V_{Ae}\right)$ (2.5×10^{-4}) is fixed, the n_b / n_h only shows a slightly negative correlation with θ.

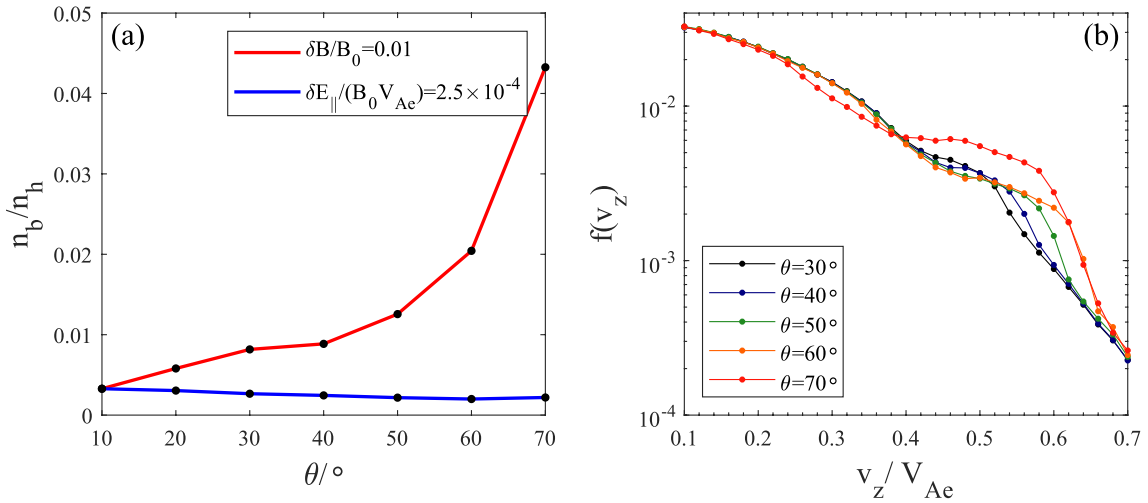

Figure 5. (a) Dependence of the ratio n_b / n_h on wave normal angle. The red line and the blue line represent $\delta B = 0.01B_0$ and $\delta E_{\parallel} / \left(B_0 V_{Ae}\right) = 2.5 \times 10^{-4}$, respectively. (b) The electron parallel velocity distributions of the cases with $\delta B = 0.01B_0$ and $\theta = 30^{\circ}, 40^{\circ}, 50^{\circ}, 60^{\circ}$, and 70°.

Figure 6 presents the estimated n_b / n_h in the (δB / B_0, θ) plane for different frequencies. As expected, for the $0.25\Omega_{ce}$ whistler mode wave, the n_b / n_h is positively correlated with δB / B_0, with the largest value of n_b / n_h = 0.1227 at δB / B_0 = 0.02 and $\theta = 70^{\circ}$ (Figure 6a). With the increase of wave frequency, the n_b / n_h also becomes larger if fixing the δB / B_0 and θ, which is due to the stronger parallel electric field for larger-frequency whistler mode waves. It is worth noting that the largest θ of whistler mode wave is limited by the resonant angle, which is estimated as $\theta_R = arc\cos\left(\omega / \Omega_{ce}\right)$.

We have also compared the simulation results with satellite observations. Since whistler mode waves typically have a finite bandwidth in the Earth's magnetosphere, we have decomposed the observed spectrum into several monochromatic whistler mode waves. The waveform data with a time interval of 6–8 s from THEMIS E satellite are utilized. Here, we present an example of wave decomposition in Figure 7, including the (a) wave magnetic field amplitude, (b) wave electric field amplitude and (c) wave normal angle as a function of frequency at 21:09:35 UT on February 26, 2011 when the wave magnetic power is strongest. The gray dashed line in panel (a) marks the amplitude threshold of 5 pT, and the selected whistler mode waves (blue dots) should be larger than 5 pT. Here, the frequency resolution of the magnetic spectrum is ~15 Hz. In this case, there are seven whistler mode waves with an amplitude above the threshold, so the initial waves in our model are their superposition. The magnetic and electric fields of whistler waves are captured

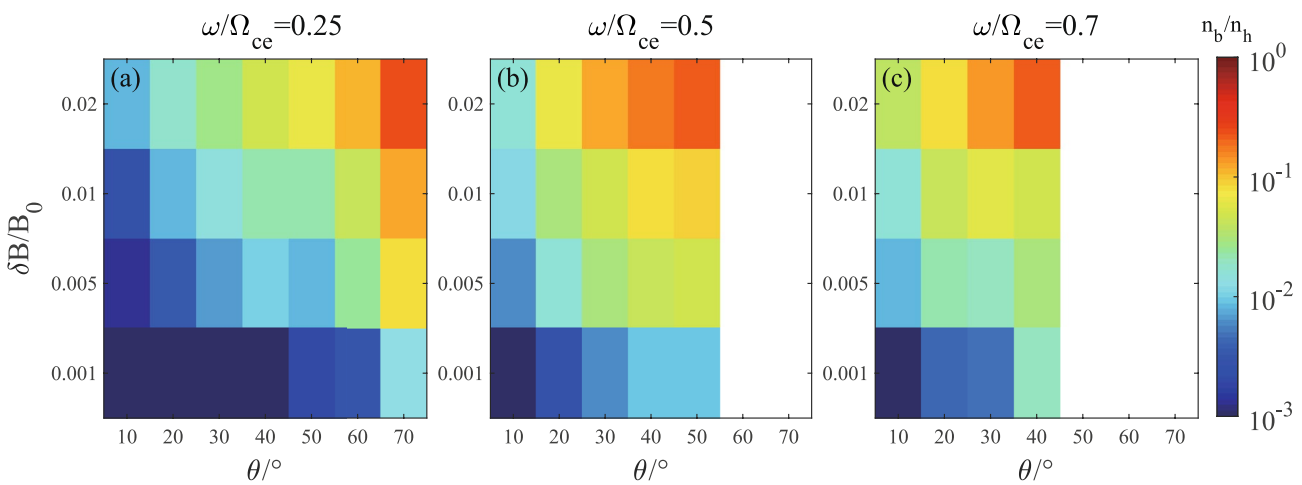

Figure 6. The value of n_b / n_h in the (δB / B_0,θ /°) plane for frequency of whistler mode wave (a) $\omega = 0.25\Omega_{ce}$, (b) $\omega = 0.5\Omega_{ce}$, and (c) $\omega = 0.7\Omega_{ce}$. The color bar represents value of n_b / n_h.

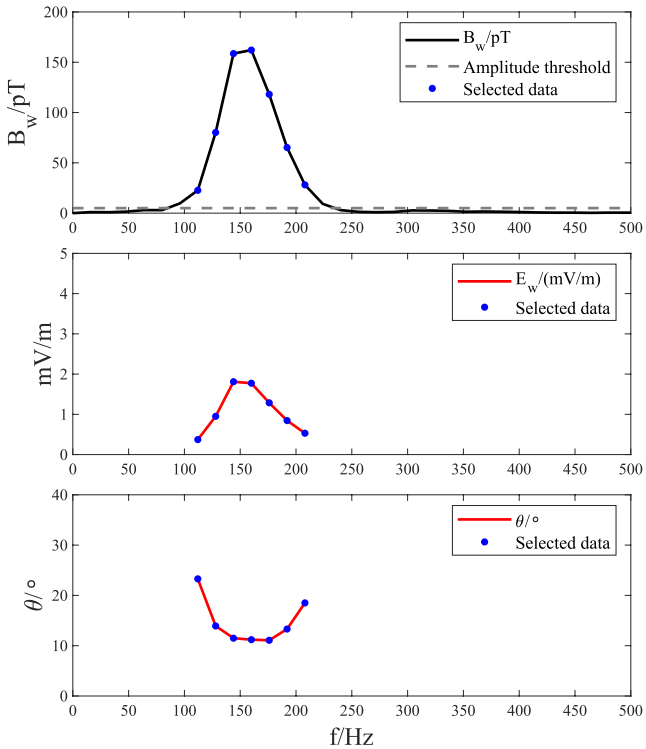

Figure 7. (a) The wave magnetic field amplitude B_w, (b) electric field amplitude E_w, and (c) wave normal angle θ as a function of frequency observed by THEMIS E at 21:44:55 on Jan 17, 2011. The blue dot represents the frequency points we selected. The gray dashed line in panel (a) represents the amplitude threshold.

by the Search-Coil Magnetometer (SCM) (Le Contel et al., 2008; Roux et al., 2008) and the Electric Field Instrument (EFI) (Bonnell et al., 2008), respectively. The plasma parameters T_h and n_h / n_0 are obtained from the electron velocity distribution provided by the Electro-Static Analyzer (ESA) (McFadden et al., 2008) onboard THEMIS over a similar time period as wave amplitudes. We use the electron thermal speed and the spacecraft potential to infer the total electron density that is utilized to estimate the plasma frequency ω_{pe} (Li et al., 2010). The electron gyrofrequency Ω_{ce} is evaluated by the background magnetic field, which is collected by the Fluxgate Magnetometer (FGM) (Auster et al., 2008). Despite the wave fields are captured by SCM and EFI onboard THEMIS, they are still limited to one point in space. If we are to study the possible resonant interactions between the particles and waves, we need its temporal and spatial description. We can obtain the fully analytical, temporal, and spatial model of the wave, using Equations 1 and 2. The values of $|\mathbf{B}w|$ and $|\mathbf{E}w|$ is set as the observed amplitudes. In this case, the simulated proportion of the beam-like population is estimated as n_b / n_h = 0.0031, which is larger than that (~0.0019) estimated from the data. We define the difference between them as δn_b / $n_h = \left[\frac{n_b / n_{hsim}}{n_b / n_{hob}} - 1\right] \times 100\%$, where $\left(n_b / n_h\right)_{sim}$ and $\left(n_b / n_h\right)_{ob}$ are the proportion of beam-like population estimated from the simulation model and satellite observation, respectively. In this case, $\delta\left(n_b / n_h\right) = 63\%$.

With this method, we have analyzed whistler mode wave events during 1 year (2011) without any preference. During this period, there are 110 quasi-parallel cases with $\theta_{avg} < 45^{\circ}$, and 57 oblique cases with $\theta_{avg} > 45^{\circ}$, where θ_{avg} represents the power-weighted average wave normal angle (Chen et al., 2019). Figure 8 shows the histograms of $\delta\left(n_b / n_h\right)$ for the (a) quasi-parallel cases and (b) oblique cases. For the quasi-parallel waves, there are 49 cases with $\left(n_b / n_h\right)_{sim}$ larger than $\left(n_b / n_h\right)_{ob}$, 16 cases with $\left(n_b / n_h\right)_{sim}$ relatively lower than $\left(n_b / n_h\right)_{ob}$, and 45 cases with $\left(n_b / n_h\right)_{sim}$ much lower than $\left(n_b / n_h\right)_{ob}$. The $\left(n_b / n_h\right)_{sim}$ can be considered as the upper limit of beam-like electron proportion formed by whistler mode

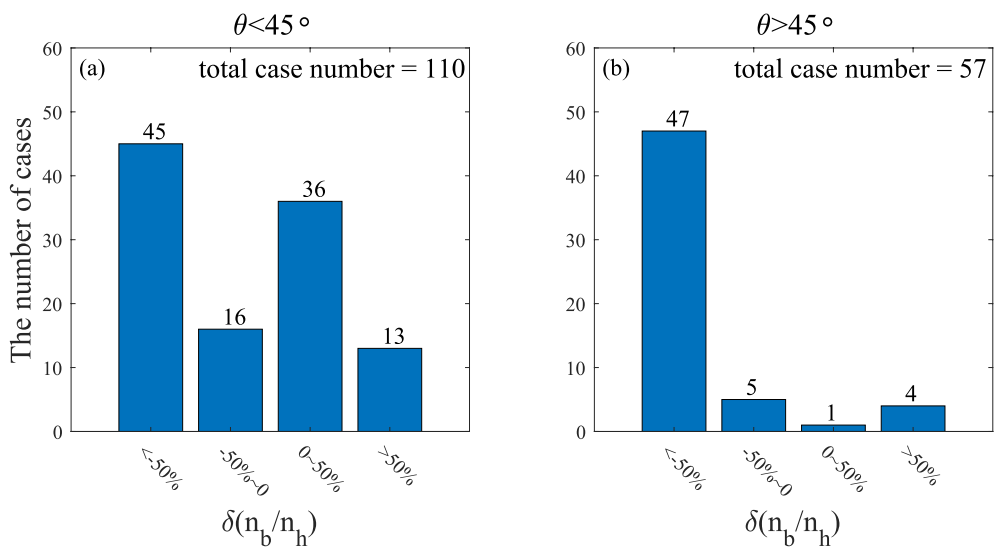

Figure 8. The number of cases corresponding to different $\delta\left(n_b / n_h\right)$ for the (a) quasi-parallel waves with $\theta_{avg} < 45^{\circ}$ and (b) oblique waves with $\theta_{avg} > 45^{\circ}$, where θ_{avg} represents the power-weighted average wave normal angle.

waves, so there are 44.5% (49 of 110) cases with the positive $\delta\left(n_b / n_h\right)$, suggesting the beam-like electrons could be due to Landau resonance with whistler mode waves. For other 55.5% cases with the negative $\delta\left(n_b / n_h\right)$, the beam-like population should be caused by other processes rather than coexisting whistler mode waves. In contrast, in the case of oblique waves, the estimated $\left(n_b / n_h\right)_{sim}$ is generally much lower than $\left(n_b / n_h\right)_{ob}$, revealing that the beam-like population is not formed by simultaneously observed waves, but is a prerequisite for the excitation of oblique waves

4. Summary and Discussion

In this paper, we have investigated the formation of beam-like electron population caused by the Landau resonance between whistle-mode waves and electrons with a test particle simulation model. The proportion of the beam-like electrons n_b / n_h has been quantified by fitting the parallel velocity distribution. There is a trend that n_b / n_h first increases and then decreases with the increase of either the temperature T_h of hot electrons or the ratio $\omega_{pe} / \Omega_{ce}$ of plasma frequency to electron gyrofrequency. In addition, n_b / n_h is positively correlated with the parallel electric field $\delta E_{\parallel} / \left(B_0 V_{Ae}\right)$, magnetic amplitude $\delta B / B_0$, wave normal angle θ, or frequency ω / Ω_{ce} of whistler mode wave if other parameters are fixed. Among all these parameters, the $\delta E_{\parallel} / \left(B_0 V_{Ae}\right)$ is found to be the most important parameter to determine n_b / n_h. Furthermore, we have also compared simulation results with THEMIS observations for one year. For quasi-parallel wave ($\theta < 45^{\circ}$) cases, there are about 44.5% (49 of 110) cases with the observed proportion $\left(n_b / n_h\right)_{ob}$ smaller than simulated one $\left(n_b / n_h\right)_{sim}$, suggesting whistler mode waves are capable of producing the observed beam-like population. While, for the other 61 cases, the $\left(n_b / n_h\right)_{ob}$ is larger than $\left(n_b / n_h\right)_{sim}$, so the beam-like components are not likely to be generated by the simultaneously observed waves. This scenario is quite common in the case of oblique waves ($\theta > 45^{\circ}$), and for nearly all of such cases the beam-like proportion is larger in observations than in the corresponding simulations.

It is worth noting that the wave amplitude is measured by THEMIS in the same latitudinal range (within $\sim 15^{\circ}$ of the geomagnetic equator) where Landau resonance with low energy (keV) electrons occurs and forms the beam-like population. During electron acceleration through Landau resonance, the wave loses energy to electrons, but this loss can be partly balanced by the free energy simultaneously provided by temperature anisotropy (Kennel & Petschek, 1966; Li et al., 2010), keeping the wave amplitude at a similar level. But during wave propagation away from the equator, wave damping often overtakes wave growth above 10° to 15°, leading to lower whistler wave amplitudes than near the equator in both observations and simulations (Agapitov et al., 2015; Lu et al., 2019). Therefore, using a constant wave amplitude should provide a good estimate of the maximum density of the beam-like electron population potentially formed by Landau resonance with the measured wave. Moreover, we have also estimated the propagation distance of whistler-mode wave when the beam-like population formed by Landau resonance reaches saturation. We find that whistler-mode wave can only propagate a distance corresponding to the magnetic latitude of 1° to 3°. Therefore, the propagating effect and change of local plasma parameters are not significant in our study. Here, the test-particle method is chosen just for saving the computation cost. Moreover, it is more convenient to study the dependences of the proportion of beam-like electrons on wave and plasma parameters.

Satellite observations reveal that whistler mode waves are usually observed along with a beam-like electron distribution near the Landau resonant velocity (Chen et al., 2019; Min et al., 2014), but the generation mechanism of the beam-like electron population is still under debate. Chen et al. (2019) found the proportion of beam-like electrons is proportional to the wave parallel electric field for quasi-parallel whistler waves, but nearly independent for quite oblique waves. So, they proposed that the beam-like electrons could result from Landau resonance in the case of quasi-parallel whistler-mode waves, but that they may be produced by other processes and provide a precondition for wave excitation in the case of very oblique waves. However, Artemyev and Mourenas (2020) pointed out that most of these beam-like electrons are unlikely to be caused by these simultaneously observed whistler waves based on the energy conservation and entropy growth laws. Based on a test particle simulation model, we have quantified the proportion of beam-like electron population that is produced by Landau resonance with whistler mode waves. The comparison between simulations and observations reveals that for some (~44.5% in this study) quasi-parallel whistler mode waves, the observed beam-like electron population could be explained by the Landau resonance. But, we

Table 1
The Fitting Parameters of the Electron Parallel Velocity Distribution for Case 1 and Case 2 Shown in Figures 2a and 2b

	n_b / n_h	T_b / eV	T_h / eV	v_d / V_{Ae}
Case 1	8.14×10^{-3}	35.7	904.4	0.4949
Case 2	2.04×10^{-2}	147.1	839.8	0.5473

find that for some quasi-parallel wave events (about 55.5%) and for nearly all oblique wave events, the beam-like electron population is unlikely to have been generated by the observed waves (Artemyev & Mourenas, 2020; Chen et al., 2019). This beam-like population could serve as a prerequisite for exciting whistler waves (Chen et al., 2019; Li et al., 2016; Mourenas et al., 2015). Our study provides new insights into the formation mechanisms of beam-like electron distribution in the Earth's magnetosphere.

Appendix A: Motion Equation of Electrons

The electron motion is controlled by the Lorentz force, which can be described by the following equations:

$$m_e \frac{d\mathbf{v}}{dt} = -e\left[\mathbf{E}_w + \mathbf{v}\times\left(\mathbf{B}_w + \mathbf{B}_0\right)\right], \tag{A1}$$

$$\frac{d\mathbf{r}}{dt} = \mathbf{v}. \tag{A2}$$

Appendix B: Method of Fitting the Distribution Function

We fit the simulated distribution function by utilizing the least square method. The fitting parameters are listed in Table 1. The parameter R^2 is the coefficient of determination, which is defined as $R^2 = 1 - SSE / SST$ (where SSE is the sum of squares of the difference between the fitting result and the measurements and SST is the sum of squares of the difference between the observed value and the average value). Here, R^2 is close to 1 meaning the fitting is reliable. In this study, we require the coefficient of determination should be larger than 0.9. This procedure for estimating the proportion (n_b / n_h) of the beam-like population is same as that used by Chen et al. (2019). In Case 1, the proportion is estimated as n_b / $n_h = 8.14\times10^{-3}$, and n_b / $n_h = 2.04\times10^{-2}$ in Case 2.

Data Availability Statement

The simulation data are archived in https://dx.doi.org/10.12176/01.99.00377. The THEMIS data used here are obtained from http://themis.ssl.berkeley.edu/data/themis.

Acknowledgments
This work was supported by the NSFC grant 41774151, 41631071, Fundamental Research Funds for the Central Universities (WK3420000013, YD3420002001), and B-type Strategic Priority Program of the Chinese Academy of Sciences, Grant No. XDB41000000. We acknowledge the data resources from National Space Science Data Center, National Science & Technology Infrastructure of China (http://www.nssdc.ac.cn). We also acknowledge the entire THEMIS instrument group.

References

Agapitov, O. V., Artemyev, A. V., Mourenas, D., Krasnoselskikh, V., Bonnell, J., Contel, O. L., et al. (2014). The quasi-electrostatic mode of chorus waves and electron nonlinear acceleration. *Journal of Geophysical Research: Space Physics*, *119*, 1606–1626. https://doi.org/10.1002/2013ja019223

Agapitov, O. V., Artemyev, A. V., Mourenas, D., Mozer, F. S., & Krasnoselskikh, V. (2015). Nonlinear local parallel acceleration of electrons through Landau trapping by oblique whistler mode waves in the outer radiation belt. *Geophysical Research Letters*, *42*, 10,140–110,149. https://doi.org/10.1002/2015gl066887

Agapitov, O. V., Mourenas, D., Artemyev, A. V., & Mozer, F. S. (2016). Exclusion principle for very oblique and parallel lower band chorus waves. *Geophysical Research Letters*, *43*, 11,112–11,120. https://doi.org/10.1002/2016gl071250

Artemyev, A. V., & Mourenas, D. (2020). On whistler mode wave relation to electron field-aligned plateau populations. *Journal of Geophysical Research: Space Physics*, *125*, e2019JA027735. https://doi.org/10.1029/2019ja027735

Auster, H. U., Glassmeier, K. H., Magnes, W., Aydogar, O., Baumjohann, W., Constantinescu, D., et al. (2008). The THEMIS Fluxgate Magnetometer. *Space Science Reviews*, *141*, 235–264. https://doi.org/10.1007/s11214-008-9365-9

Bonnell, J. W., Mozer, F. S., Delory, G. T., Hull, A. J., Ergun, R. E., Cully, C. M., et al. (2008). The Electric Field Instrument (EFI) for THEMIS. *Space Science Reviews*, *141*, 303–341. https://doi.org/10.1007/s11214-008-9469-2

Bortnik, J., & Thorne, R. M. (2007). The dual role of ELF/VLF chorus waves in the acceleration and precipitation of radiation belt electrons. *Journal of Atmospheric and Solar-Terrestrial Physics*, *69*(3), 378–386. https://doi.org/10.1016/j.jastp.2006.05.030

Burtis, W. J., & Helliwell, R. A. (1969). Banded chorus-A new type of VLF radiation observed in the magnetosphere by OGO 1 and OGO 3. *Journal of Geophysical Research*, *74*(11), 3002–3010. https://doi.org/10.1029/JA074i011p03002

Chen, H., Gao, X., Lu, Q., Sauer, K., Chen, R., Yao, J., & Wang, S. (2021). Gap Formation Around 0.5Ωe of Whistler-Mode Waves Excited by Electron Temperature Anisotropy. *Journal of Geophysical Research: Space Physics*, *126*. https://doi.org/10.1029/2020ja028631 e2020JA028631.

Chen, H., Sauer, K., Lu, Q., Gao, X., & Wang, S. (2020). Two-band whistler-mode waves excited by an electron bi-Maxwellian distribution plus parallel beams. *AIP Advances*, *10*, 125010. https://doi.org/10.1063/5.0026220

Chen, L., Thorne, R. M., Li, W., & Bortnik, J. (2013). Modeling the wave normal distribution of chorus waves. *Journal of Geophysical Research: Space Physics*, *118*, 1074–1088. https://doi.org/10.1029/2012ja018343

Chen, R., Gao, X., Lu, Q., & Wang, S. (2019). Unraveling the correlation between chorus wave and electron beam-like distribution in the Earth's magnetosphere. *Geophysical Research Letters*, *46*, 11671–11678. https://doi.org/10.1029/2019gl085108

Demekhov, A. G., Taubenschuss, U., & Santolík, O. (2017). Simulation of VLF chorus emissions in the magnetosphere and comparison with THEMIS spacecraft data. *Journal of Geophysical Research: Space Physics*, *122*(1), 166–184. https://doi.org/10.1002/2016ja023057

Gao, X., Ke, Y., Lu, Q., Chen, L., & Wang, S. (2017). Generation of multiband chorus in the Earth's magnetosphere: 1-D PIC simulation. *Geophysical Research Letters*, *44*(2), 618–624. https://doi.org/10.1002/2016gl072251

Gao, X., Li, W., Thorne, R. M., Bortnik, J., Angelopoulos, V., Lu, Q., et al. (2014). New evidence for generation mechanisms of discrete and hiss-like whistler mode waves. *Geophysical Research Letters*, *41*(14), 4805–4811. https://doi.org/10.1002/2014gl060707

Goldstein, B. E., & Tsurutani, B. T. (1984). Wave normal directions of chorus near the equatorial source region. *Journal of Geophysical Research*, *89*(A5), 2789–2810. https://doi.org/10.1029/JA089iA05p02789

Horne, R. B. (2003). Resonant diffusion of radiation belt electrons by whistler-mode chorus. *Geophysical Research Letters*, *30*(9), 1493. https://doi.org/10.1029/2003gl016963

Horne, R. B., & Thorne, R. M. (2003). Relativistic electron acceleration and precipitation during resonant interactions with whistler-mode chorus. *Geophysical Research Letters*, *30*(10), 1527. https://doi.org/10.1029/2003gl016973

Kennel, C. F., & Petschek, H. E. (1966). Limit on stably trapped particle fluxes. *Journal of Geophysical Research*, *71*(1), 1–28. https://doi.org/10.1029/JZ071i001p00001

Le Contel, O., Roux, A., Robert, P., Coillot, C., Bouabdellah, A., de la Porte, B., et al. (2008). First results of the THEMIS search coil magnetometers. *Space Science Reviews*, *141*, 509–534. https://doi.org/10.1007/s11214-008-9371-y

LeDocq, M. J., Gurnett, D. A., & Hospodarsky, G. B. (1998). Chorus source locations from VLF Poynting flux measurements with the Polar spacecraft. *Geophysical Research Letters*, *25*(21), 4063–4066. https://doi.org/10.1029/1998gl900071

Li, J., Bortnik, J., An, X., Li, W., Angelopoulos, V., Thorne, R. M., et al. (2019). Origin of two-band chorus in the radiation belt of Earth. *Nature Communications*, *10*, 4672. https://doi.org/10.1038/s41467-019-12561-3

Li, W., Bortnik, J., Thorne, R. M., & Angelopoulos, V. (2011). Global distribution of wave amplitudes and wave normal angles of chorus waves using THEMIS wave observations. *Journal of Geophysical Research*, *116*, A12205. https://doi.org/10.1029/2011ja017035

Li, W., Mourenas, D., Artemyev, A. V., Bortnik, J., Thorne, R. M., Kletzing, C. A., et al. (2016). Unraveling the excitation mechanisms of highly oblique lower band chorus waves. *Geophysical Research Letters*, *43*, 8867–8875. https://doi.org/10.1002/2016gl070386

Li, W., Thorne, R. M., Angelopoulos, V., Bortnik, J., Cully, C. M., Ni, B., et al. (2009). Global distribution of whistler-mode chorus waves observed on the THEMIS spacecraft. *Geophysical Research Letters*, *36*(9), L09104. https://doi.org/10.1029/2009gl037595

Li, W., Thorne, R. M., Bortnik, J., Shprits, Y. Y., Nishimura, Y., Angelopoulos, V., et al. (2011). Typical properties of rising and falling tone chorus waves. *Geophysical Research Letters*, *38*, L14103. https://doi.org/10.1029/2011gl047925

Li, W., Thorne, R. M., Bortnik, J., Tao, X., & Angelopoulos, V. (2012). Characteristics of hiss-like and discrete whistler-mode emissions. *Geophysical Research Letters*, *39*(18). https://doi.org/10.1029/2012gl053206

Li, W., Thorne, R. M., Nishimura, Y., Bortnik, J., Angelopoulos, V., McFadden, J. P., et al. (2010). THEMIS analysis of observed equatorial electron distributions responsible for the chorus excitation. *Journal of Geophysical Research*, *115*, A00F11. https://doi.org/10.1029/2009ja014845

Lu, Q., Ke, Y., Wang, X., Liu, K., Gao, X., Chen, L., & Wang, S. (2019). Two-dimensional gcPIC simulation of rising-tone chorus waves in a dipole magnetic field. *Journal of Geophysical Research: Space Physics*, *124*, 4157–4167. https://doi.org/10.1029/2019ja026586

McFadden, J. P., Carlson, C. W., Larson, D., Ludlam, M., Abiad, R., Elliott, B., et al. (2008). The THEMIS ESA plasma instrument and in-flight calibration. *Space Science Reviews*, *141*, 277–302. https://doi.org/10.1007/s11214-008-9440-2

Min, K., Liu, K., & Li, W. (2014). Signatures of electron Landau resonant interactions with chorus waves from THEMIS observations. *Journal of Geophysical Research: Space Physics*, *119*, 5551–5560. https://doi.org/10.1002/2014ja019903

Mourenas, D., Artemyev, A. V., Agapitov, O. V., Krasnoselskikh, V., & Mozer, F. S. (2015). Very oblique whistler generation by low-energy electron streams. *Journal of Geophysical Research: Space Physics*, *120*, 3665–3683. https://doi.org/10.1002/2015ja021135

Ni, B., Thorne, R. M., Shprits, Y. Y., Orlova, K. G., & Meredith, N. P. (2011). Chorus-driven resonant scattering of diffuse auroral electrons in nondipolar magnetic fields. *Journal of Geophysical Research*, *116*(A6), A06225. https://doi.org/10.1029/2011ja016453

Omura, Y., Hikishima, M., Katoh, Y., Summers, D., & Yagitani, S. (2009). Nonlinear mechanisms of lower-band and upper-band VLF chorus emissions in the magnetosphere. *Journal of Geophysical Research*, *114*, A07217. https://doi.org/10.1029/2009ja014206

Ronnmark, K. (1982). *WHAMP: Waves in homogeneous, anisotropic, multicomponent plasmas Report No. 179*. Kiruna Geophysics Institute.

Roux, A., Le Contel, O., Coillot, C., Bouabdellah, A., de la Porte, B., Alison, D., et al. (2008). The search coil magnetometer for THEMIS. *Space Science Reviews*, *141*, 265–275. https://doi.org/10.1007/s11214-008-9455-8

Taubenschuss, U., Khotyaintsev, Y. V., Santolík, O., Vaivads, A., Cully, C. M., Contel, O. L., & Angelopoulos, V. (2014). Wave normal angles of whistler mode chorus rising and falling tones. *Journal of Geophysical Research: Space Physics*, *119*, 9567–9578. https://doi.org/10.1002/2014ja020575

Thorne, R. M. (2010). Radiation belt dynamics: The importance of wave-particle interactions. *Geophysical Research Letters*, *37*(22), L22107–n. https://doi.org/10.1029/2010gl044990

Thorne, R. M., Li, W., Ni, B., Ma, Q., Bortnik, J., Chen, L., et al. (2013). Rapid local acceleration of relativistic radiation-belt electrons by magnetospheric chorus. *Nature*, *504*(7480), 411–414. https://doi.org/10.1038/nature12889

Thorne, R. M., Ni, B., Tao, X., Horne, R. B., & Meredith, N. P. (2010). Scattering by chorus waves as the dominant cause of diffuse auroral precipitation. *Nature*, *467*(7318), 943–946. https://doi.org/10.1038/nature09467

Tsurutani, B. T., & Smith, E. J. (1974). Postmidnight chorus: A substorm phenomenon. *Journal of Geophysical Research*, *79*(1), 118–127. https://doi.org/10.1029/JA079i001p00118

Tsurutani, B. T., & Smith, E. J. (1977). Two types of magnetospheric ELF chorus and their substorm dependences. *Journal of Geophysical Research*, *82*(32), 5112–5128. https://doi.org/10.1029/JA082i032p05112